PRESEISMIC RUPTURE PROGRESSION AND GREAT EARTHQUAKE INSTABILITIES AT PLATE BOUNDARIES

Victor C. Li

Department of Civil Engineering, Massachusetts Institute of Technology
Cambridge, Massachusetts 02139

James R. Rice

Division of Applied Sciences, Harvard University, Cambridge, Massachusetts 02138

Abstract. We present a procedure for modeling the initially quasi-static upward progression of a zone of slip from some depth in the lithosphere toward the earth's surface, along a transform plate margin, culminating in a great crustal earthquake. Stress transmission in the lithosphere is analyzed with a generalized Elsasser model, in which elastic lithospheric plates undergo plane stress deformation and are coupled by an elementary foundation model to a Maxwellian viscoelastic asthenosphere. Upward progression of rupture over a finite length of plate boundary, corresponding to a seismic gap along strike, is analyzed by a method based on the 'line-spring' concept, whereby a two-dimensional antiplane analysis of the upward progression provides the relation between lithospheric thickness-averaged stress and slip used as a boundary condition in the generalized Elsasser plate model. The formulation results in a nonlinear integral equation for the rupture progression as a function of time and distance along strike. A simpler approximate single degree of freedom analysis procedure is described and shown to lead to instability results that can be formulated in terms of the slip-softening slope at the boundary falling below the elastic unloading stiffness of the surroundings. The results also indicate a delay of ultimate (seismic) instability due to the stiffer short versus long time asthenospheric response and predict a final period of self-driven creep toward instability. The procedures for prediction of rupture progression and instability are illustrated in detail for an elastic-brittle crack model of slip zone advance, and parameters of the model are chosen consistently with great earthquake slips and stress drops. For example, an effective crack fracture energy of the order 4×10^6 J/m^2 at the peak, 7 to 10 km below surface, of a Gaussian bell-shaped distribution of fracture energy with depth, with variance of the order 5 km, simulating strength build-up in a seismogenic layer, leads to prediction of nominal seismic stress drops of 30 to 60 bars and slips of 2 to 5 m in great strike slip earthquake ruptures breaking 100 to 400 km along strike. Precursory surface straining in the self-driven stage is predicted to proceed at a distinctly higher rate over time intervals beginning 3 to 10 months before such an earthquake, this interval being greater for longer distances along strike over which the preseismic upward rupture progression takes place.

Introduction

It seems plausible that zones of slip or of concentrated shear strain along a plate boundary initiate at considerable depth in the lithosphere and spread upward, in a generally aseismic manner, toward the earth's surface. Ultimately, the slipping zone must traverse the shallower parts of the crust (seismogenic layer) if overall plate motion is to occur, and this traversal is sometimes accomplished in the form of a great crustal earthquake. The concept that crustal earthquakes result from the loading of a shallow crustal zone by slip at depth has been adopted by many authors [e.g., Savage and Burford, 1973; Turcotte and Spence, 1974; Prescott and Nur, 1981]. It has been discussed particularly by Stuart [1979a, b], Stuart and Mavko [1979], Nur [1981], and Dmowska and Li [1982] in a manner that includes account of the time-dependent, initially aseismic, upward progression of a slip rupture zone, possibly terminating in a great earthquake instability, that we attempt to model in this paper.

We assume that because of the increase of pressure and temperature with depth, plate boundary slip, or concentrated shear deformation, can be accomplished in the mid-lithosphere and lower lithosphere without the requirement that some significant strength barrier to deformation first be overcome, that is, without a significant strength drop with ongoing slip. In contrast, the upper crust responds in a brittle manner. In many regions of the earth, it remains effectively locked until some large stress builds up to initiate slip, and then slip proceeds at what one infers to be a lower strength level. This lowering, with ongoing slip, of the stress required to sustain slip allows the possibility of earthquake instabilities, provided that the elastic stiffness of the fault surroundings is sufficiently low.

Different models have been constructed to study the various phases of the earthquake cycle, including elastic strain accumulation, coseismic release, and postseismic readjustment. A realistic model for the study of the strain accumulation phase, and particularly for the study of related effects precursory to a major earthquake, should take into account the possibility of aseismic slip zone progression, since such progression not only alters surface deformation but also causes the unslipped ligament to carry an increasing amount of tectonic load. Hence physical processes associated with (rapid) loading
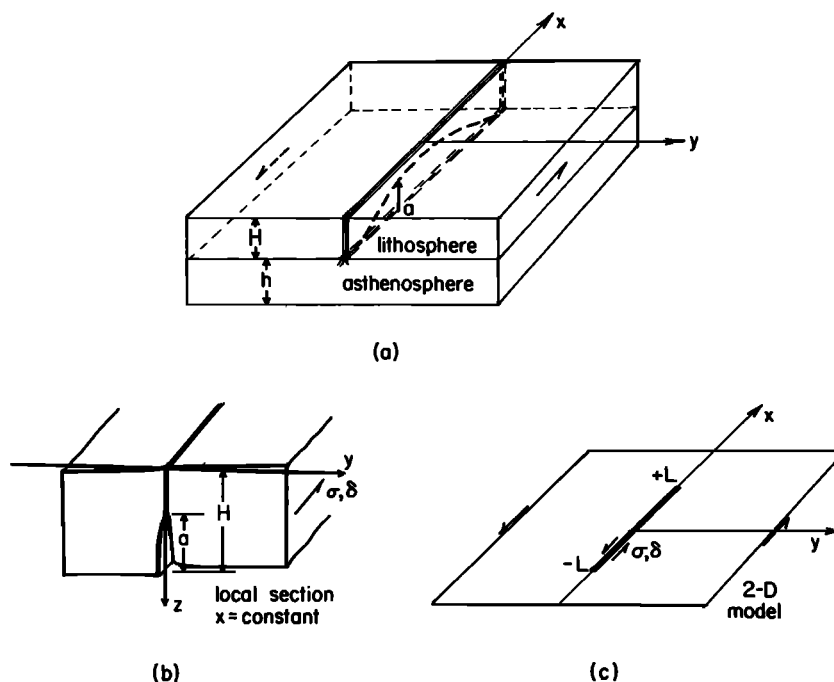
Fig. 1. (a) Upward quasi-static progression of a slip rupture at a seismic gap zone along a transform plate boundary. (b) Two-dimensional antiplane model of rupture progression; provides basis for relation of equation (10) between thickness-averaged stress σ and slip δ at the section x = const. (c) Two-dimensional generalized Elsasser plane stress model of elastic lithospheric plate coupled to Maxwellian viscoelastic asthenosphere; discontinuity over -L < x < +L corresponds to gap zone over which rupture is occurring.

rate would manifest themselves as a result of the spreading of such a slip zone.

Stuart [1979a] and Stuart and Mavko [1979] postulate a slip-weakening relation between shear strength and slip displacement on the fault and analyze two-dimensional problems of indefinitely long antiplane strain (mode III) strike slip faults in a lithospheric plate (e.g., as in Figure 1b). Stuart [1979b] also presented an analogous study of plane strain (mode II) slip for thrust faulting. Their relation of strength to slip is chosen to exhibit the greatest potential strength drop at the center of a bell-shaped strength distribution, where the peak of the distribution is assumed to lie in the seismogenic layer, e.g., at depths of order 10 km. Stuart and Mavko [1979] enforce displacement boundary conditions at the sides of a region like that shown in Figure 1b in a manner intended to simulate remotely imposed plate motions and calculate the progression of slip with increasing displacement. Depending on whether the strength drop in slip weakening occurs with relatively large or small amounts of displacement, the slip process may take place simultaneously over the entire plate boundary or may involve the cracklike progression of a single slipping zone or zones. Dynamic, seismic instability occurs when, and if, the effective, overall slip-softening slope (in a plot of thickness-averaged stress versus thickness-averaged slip at the rupturing plate boundary) falls below the elastic unloading stiffness of the adjoining plates.

While procedures in such modeling seem sound

from the standpoint of basic rupture mechanics, the models addressed do not include two significant features of the tectonic environment. We discuss these with reference to Figure 1a, and our work here aims at approximate inclusion of both. First, the surface trace along the plate boundary of the region active in a given great earthquake rupture is finite, of length of the order of only a few lithospheric thicknesses. For example, Sykes and Quittmeyer [1981] and Scholz [1982] tabulate rupture lengths in 14 great strike slip earthquakes that range from 30 to 450 km and in 12 recent (1952 to 1978) great thrust ruptures that range from 80 to 1000 km. The length is, presumably, often dictated by the size of a high stress zone or series of zones isolated, as a seismic gap, by previous ruptures of adjacent portions of the plate boundary; why plate boundary rupture occurs in this heterogeneous mode is not of itself fully understood. The second feature of the tectonic environment which has not been fully accounted for in the models discussed is that the lithosphere is coupled to the rest of the earth, in particular, to the astehenosphere and mantle at its base. Such coupling may presumably be neglected because of viscous relaxation in the asthenosphere on long time scales, perhaps comparable to earthquake repeat times. But the coupling must be important on the relatively short time scale of events leading up to instability. (Stuart and Mavko [1979] do take some account of this coupling by comparing their results to those of a calculation by Stuart [1979a] for which rigid

displacement boundary conditions are imposed at the base of the lithospheric plate as well as at its sides.)

A previous attempt to allow for the finite surface trace of the rupture and, at the same time, a different perspective on modeling of aseismic slip progression has been given by Nur [1981]. He proposes an upward propagating dislocation segment, pinned low in the lithosphere at the ends of the region to be ruptured and accomplishing slip of constant Burgers vector in a strike slip mode. The dislocation moves under action of the applied stress and an attractive image stress; this image stress becomes indefinitely large as the dislocation line comes near to the earth surface. Nur represents the retarding effect of the finite length of the dislocation segment by a line tension approximation. While the model thus involves an attempt to include finite along strike length of the rupture, it does not include coupling to an asthenosphere of time-dependent rheology.

Nur's method of representing slip progression, by upward motion of a single, constant slip dislocation, is not developed to the point where contact can be made with some constitutive relation between stress and slip on the rupturing surface. However, the approach does potentially represent an opposite limiting case to the slip-weakening model used by Stuart [1979a, b] and Stuart and Mavko [1979]. In the latter, once slip of sufficient magnitude has occurred, strength is degraded and all subsequent slip takes place at the degraded strength level; there is no healing or other strength recovery. By contrast, the constant slip dislocation model can perhaps be thought of as representing approximately an opposite extreme, in which rehealing to full, coherent strength follows very quickly after progression of a slip offset.

To summarize the modeling concepts which we present here, great plate boundary earthquakes are analyzed as instabilities in the upward progression of zones of slip or of concentrated shear from some depth in the lithosphere toward the earth's surface (Figure 1a). The precise manner of representing the local physics of rupture progression, whether according to a slip-weakening model or a dislocation model or an as yet not well-developed model inclusive of slip weakening, healing, and possibly other rate or time effects on the fault surface, can be left open as regards the general description of our procedure. We do, however, illustrate it later by specific calculations for an elastic-brittle crack model of rupture progression, which can be regarded as a limiting case of the slip-weakening approach, valid when strength degrades significantly with only a small amount of slip. In the case of a transform boundary as we consider here (Figure 1a), slip zone progression at every vertical slice x = const is modeled as the advance, under local two-dimensional antiplane strain conditions, of a mode III rupture in an elastic strip (Figure 1b). The strip is identified as the elastic lithosphere, and the rupture advances into a region of nonuniform fracture resistance, having greatest potential strength drop in the seismogenic layer. Stress transmission in the lithosphere itself is analyzed by a generalized Elsasser model, in which elastic

plates sustain plane stress deformation and are coupled at their base in an elementary way to a Maxwellian viscoelastic asthenosphere; this lithospheric model was introduced by Rice [1980] and further developed by Lehner et al. [1981]. Of course, actual slip zone progression of a geometry as illustrated in Figure 1a provides a complicated three-dimensional problem. Our method in this paper is to retain its essential features but to reduce it to a more tractable two-dimensional plane stress problem for the generalized Elsasser plate, in which the progression of the slip zone enters as a nonlinear boundary condition relating thickness-averaged stress to thickness-averaged slip along the trace, in the two-dimensional plate mode (Figure 1c), of the ruptured boundary. Full details are given in the next section. The procedures are similar to those of the 'line spring' model of fracture mechanics [Rice and Levy, 1972; Rice, 1972], used widely for the analysis of part-through surface cracks in elastic plates or shells; see Parks et al. [1981], Parks [1981], and Delale and Erdogan [1982] as examples of recent applications.

Our analysis of the model described shows that instability occurs, if at all, when the rupturing zone has advanced such that the lithospheric thickness-averaged stress at the rupturing boundary is decreasing at a critical rate with ongoing thickness-averaged slip. This critical rate is equal to an appropriately defined elastic unloading stiffness of the lithosphere-asthenosphere system. The stiffness is greater for short-time response, in which the asthenosphere responds elastically, than for long-time response in which the asthenosphere is relaxed. Hence once the instability point corresponding to a relaxed asthenosphere is passed, the system enters a self-driven state and proceeds toward final (dynamic) instability at a rate controlled by plate boundary rupture resistance properties and by asthenospheric rheology. Although thickness-averaged stresses decrease as instability approaches, the continual advance of the slip zone leads to nonlinearly increasing stress at the earth's surface along the soon-to-be ruptured trace of plate boundary.

Our rupture modeling procedures extend the type of work reported, e.g., by Stuart [1979a, b] and Stuart and Mavko [1979], by adding a more realistic assessment of the tectonic conditions, notably by incorporating finiteness in along-strike length of the rupturing region, possibly due to stress heterogeneity, and especially by including the effects of lithospheric coupling to a viscoelastic asthenosphere.

Stress Transmission and Rupture Progression in a Coupled Elastic Lithosphere and Viscoelastic Asthenosphere

To model the interaction of the lithosphere with a viscously relaxing asthenosphere, we adopt a model in the spirit of Elsasser's [1969] but generalized as in recent work of Rice [1980] and Lehner et al. [1981]. This model treats the lithosphere as an elastic plate of thickness H which can undergo general elastic 'plane stress' deformations and which rides on a Maxwellian viscoelastic asthenosphere to which it is coupled in an elementary way. Hence if x,y are coordi-

nates in the plane of the plate and σ_{xx}, σ_{xy}, σ_{yy} are the thickness-averaged in-plane stress components, i.e.,

$$\sigma_{ij}(x,y,t) = \frac{1}{H} \int_0^H \tau_{ij}(x,y,z,t) \, dz \qquad i,j=x,y \qquad (1)$$

where $\tau_{ij}(x,y,z,t)$ denotes the three-dimensional stress distribution, equilibrium requires that

$$\partial\sigma_{ix}/\partial x + \partial\sigma_{iy}/\partial y = \tau_i/H \qquad i=x,y \qquad (2)$$

where $\tau_i = -\tau_{zi}(x,y,H,t)$ is the resistive shear shear stress at the base of the lithosphere. The plate model is completed by assumption of the following constitutive relations between σ_{ij}, τ_i and the thickness-averaged (like for σ_{ij} in (1) above) in-plane displacements $u_i = u_i(x,y,t)$; here $i,j = x,y$. First, thickness-averaged in-plane stress and strain components are related to one another in the manner appropriate for states of elastic plane stress,

$$\sigma_{ij} = G\left(\frac{\partial u_i}{\partial j} + \frac{\partial u_j}{\partial i} + \frac{2\nu}{1-\nu}\delta_{ij}\sum_{k=x,y}\frac{\partial u_k}{\partial k}\right) \qquad (3)$$

where $i,j = x,y$, δ_{ij} is the Kronecker delta and G and ν are the elastic shear modulus and Poisson ratio for the lithosphere. Second, in the spirit of elementary foundation models, a Maxwell coupling of τ_i to u_i is postulated,

$$\frac{\partial u_i}{\partial t} = \frac{b}{G}\frac{\partial \tau_i}{\partial t} + \frac{h}{\eta}\tau_i \qquad (4)$$

Here $i = x,y$, h can be interpreted as the thickness of an asthenosphere of uniform viscosity η, and [see Lehner et al., 1981] an appropriate estimate of b is $b \approx (\pi/4)^2 H$ if the elastic shear modulus of the asthenosphere is also approximately equal to G. By substituting these constitutive equations into the equilibrium equation one obtains as governing equations for the thickness-averaged displacement field

$$\left(\alpha + \beta\frac{\partial}{\partial t}\right)\sum_{k=x,y}\left(\frac{\partial^2 u_j}{\partial k^2} + \frac{1+\nu}{1-\nu}\frac{\partial^2 u_k}{\partial k\partial j}\right) = \frac{\partial u_j}{\partial t} \qquad (5)$$

for $j = x,y$, where $\alpha = hHG/\eta$ and $\beta = bH$. Note that $\beta/\alpha = (\eta/h)/(G/b)$ is the characteristic relaxation time of the viscoelastic foundation. Choosing $h = 100$ km [Cathles, 1975; Stacey, 1977], $G = 5.5 \times 10^{10}$ Pa as a lithosphere average shear modulus [Stacey, 1977], $H = 75$ km as a representative thickness of the lithosphere, and $\eta = 2.0 \times 10^{19}$ Pa s as the viscosity of the foundation (see the discusion of different estimates by Lehner et al. [1981]), and by using $b \approx (\pi/4)^2 H$, the relaxation time $\beta/\alpha \approx 5$ years.

It is, in general, too complicated to solve the two coupled equations represented by (5). Lehner et al. [1981] show that for purposes such as those that we have here, namely, of relating thickness averaged slip motions

$$\delta(x,t) \equiv u_x(x,0^+,t) - u_x(x,0^-,t) \qquad (6)$$

to shear stress alterations

$$\sigma(x,t) \equiv \sigma_{xy}(x,0,t) \qquad (7)$$

along a strike slip plate boundary, the simpler physically motivated model equation

$$\left(\alpha + \beta\frac{\partial}{\partial t}\right)\left[(1+\nu)^2\frac{\partial^2 u_x}{\partial x^2} + \frac{\partial^2 u_x}{\partial y^2}\right] = \frac{\partial u_x}{\partial t} \qquad (8)$$

may be used with associated shear stress given by $\sigma_{xy} = G\,\partial u_x/\partial y$. Lehner et al. [1981] demonstrate that solutions to the model equation (8) reproduce closely solutions to the more exact coupled set (5) relating arbitrary slip distributions $\delta(x,t)$ to associated stress distributions $\sigma(x,t)$ and do so exactly in the limits of short and long spatial wavelength disturbances as well as for all wavelengths when the foundation is relaxed. This was demonstrated by calculating the ratio of $D(\omega,s)$ to $\Sigma(\omega,s)$, where these are the Fourier and Laplace transformations of $\delta(x,t)$ and $\sigma(x,t)$, respectively, from both the model equation (8) and the exact set (5). The ratio D/Σ from (8) was shown to be numerically close to that from (5) for all real ω and s, and the ratios were shown to coincide exactly in the limits discussed. hence no significant error is introduced by using (8) rather than (5) as a basis for relating $\delta(x,t)$ to $\sigma(x,t)$.

To emphasize that stress transmission in the lithospheric plate is being modeled by a two-dimensional theory, dealing only with thickness averages of stress and displacement, we have redrawn the three-dimensional configuration of Figure 1a as the two-dimensional surface in the x,y plane shown in Figure 1c. The rupturing plate boundary appears as a line of discontinuity extending over $-L < x < +L$ in this two-dimensional surface, where we assume that upward progression of rupture in a given earthquake sequence occurs over the along-strike segment of length 2L.

The completion of our formulation requires combination in the spirit of the 'line spring' model of two inputs. The first comes from the generalized Elsasser model just discussed. Recognizing that this model is linear, it is clear that solutions to (5) or (8), relating arbitrary slip distributions $\delta(x,t)$ to alteration of stress $\sigma(x,t)$, can be put in the form

$$\sigma(x,t) = \sigma_0(x,t)$$
$$- \int_{-\infty}^{t}\int_{-L}^{+L} g(x-x',t-t')\frac{\partial^2\delta(x',t')}{\partial x'\partial t'}\,dx'\,dt' \qquad (9)$$

where $\sigma_0(x,t)$ is the stress that would be transmitted to the boundary in the absence of slip (i.e., if $\delta = 0$), due to overall tectonic processes resulting in remote plate motions, and where $g(x,t)$ is an appropriate Green's function. In fact, $g(x,t)$ is the thickness-averaged shear stress at x,t due to sudden introduction at $t = 0$ of a dislocation in thickness-averaged slip of unit Burgers vector over $-\infty < x < 0$. The explicit form for $g(x,t)$ is not necessary for our present purposes, but it can be developed by solution

methods of Lehner et al. [1981] and has been given by Li [1981].

The second input comes from the modeling of rupture progression in the two-dimensional antiplane strain configuration of Figure 1b. Because of this rupture progression, the thickness-averaged stress σ transmitted across the boundary in Figure 1b can be regarded as a function of (or functional of, for time- or rate-dependent constitutive response in the rupture zone) the thickness-averaged slip δ. Symbolically, σ = f(δ), and we show how to construct explicitly this relation for the elastic-brittle crack model of rupture progression two sections henceforth. We therefore assume that the thickness averages σ(x,t) and δ(x,t) at any section x = const along the rupturing plate boundary are related to one another in the same way, namely,

$$\sigma(x,t) = f[\delta(x,t),x] \tag{10}$$

which is understood to be based on the antiplane strain analysis depicted in Figure 1b, using the distribution of fracture or slip constitutive properties with depth z as appropriate for the slice x = const. Hence the explicit x dependence in (10) allows for possible nonuniformity along strike of the distribution of fracture properties with depth, and Dmowska and Li [1982] remark that such an explicit dependence allows the modeling of strength asperities.

The heavy curve in Figure 2 shows a schematic σ versus δ relation, appropriate when rate dependence of the process of rupture progression is ignored so that the result of the underlying mode III analysis of rupture progression is to define σ as a function of δ. (The zero level for σ and σ₀ can be chosen arbitrarily; we measure σ from the stress at the end of the previous great earthquake cycle at the section of plate boundary considered.) A significant feature of the curve shown, consistent with our later modeling by elastic brittle crack theory, is that σ rises to a peak value and then decreases with increasing δ. Of course, the σ and δ shown represent averages over the lithospheric thickness; the actual local stress near the earth's surface increases significantly, according to our crack calculations, in the later stages of rupture as the slip zone grows upward toward the surface, even though the thickness-averaged σ is then decreasing.

The result of the two inputs, summarized as (9) and (10), is to provide an explicit integral equation governing the time evolution of δ(x,t) when σ(x,t) in (9) is replaced by the function or functional in (10) relating it to δ(x,t). The driving function in the integral equation is σ₀(x,t), which represents the stress that overall tectonic processes would have caused to be transmitted across the plate boundary had there been no slip δ(x,t) there.

This use of results from two two-dimensional analyses, one for plane stress in the lithospheric plate (x,y plane) and the other for mode III rupture progression (y,z planes), when combined as explained so that the latter analysis provides boundary conditions along the cut −L < x < +L in Figure 1c, is the essence of the 'line spring' procedure of Rice and Levy [1972]. Its initial development was for part-through tensile cracks
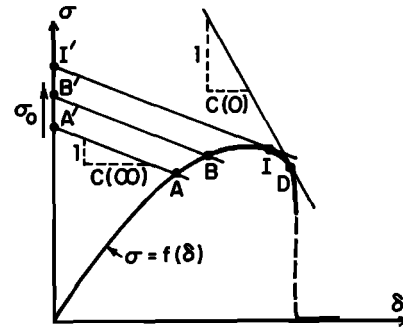

Fig. 2. Representative relation between thickness-averaged stress σ and slip δ. Constructions show determination of instability points I (instability of uncoupled lithosphere) and D (dynamic, seismic instability for coupled lithosphere-asthenosphere system) for single degree of freedom approximation.

penetrating inward from the surface of elastic plates subject to tension and bending loads relative to the crack line. In that case the line spring, representing a cut in a two-dimensional plane like that in Figure 1c, responds by both opening displacement and rotation, where these are connected by a constitutive equation to local tensile stress and bending moment; the constitutive relation is then derived from the plane strain solution for tension and bending of an edge-cracked strip. Recent applications of the model and comparisons against three-dimensional numerical crack solutions [Parks, 1981; Parks et al., 1981; Delale and Erdogan, 1982] have shown that it is remarkably accurate in determination of crack tip stress intensities, even when the surface length of the crack is of the order of plate thickness.

An essential new feature that we have introduced here is the coupling of the plate to a foundation, done with the generalized Elsasser model. We present a calculation in Appendix A which is intended to test this new feature by applying our model to the calculation of the stress intensity factor at the tip of an infinitely long (in the x direction) mode III crack, of depth ɑ, that is introduced into a lithosphere which is coupled to a wholly elastic asthenosphere of the same shear modulus. An exact solution is available also for this problem. The agreement between the two is shown to be reasonably good and hence to support our modeling procedure.

The procedure that we have outlined and summarized in (9) and (10) is rather general and is open to wide variations in the modeling of rupture as well as to generalizations of the Elsasser-like plate model described, e.g., so as to include depth-dependent linear viscoelastic rheological properties of the lithospheric plates. The full modeling procedure as outlined has, thus far, been carried through in detail [Li, 1981] only for the case in which the lithospheric plate is decoupled from the asthenosphere. In this case the plate equations revert to those of classical elastic plane stress theory, and the Green's function g(x,t) becomes time independent,

$$g(x,t) = (1+\nu)G/2\pi x \tag{11}$$

Hence, when coupling to the asthenosphere can be neglected, the integral relation of (9) becomes

$$\sigma(x,t) = \sigma_0(x,t)$$

$$- \frac{(1+\nu)G}{2\pi} \int_{-L}^{+L} \frac{1}{x-x'} \frac{\partial\delta(x',t)}{\partial x'} \, dx' \qquad (12)$$

Li [1981] used numerical procedures to generate a number of solutions for this uncoupled model, using a form $\sigma = f(\delta,x)$, as in (10), consistent with the elastic-brittle crack model that we describe two sections hence. He also examined along-strike nonuniformity of strength, reflected in an explicit x dependence of $f(\delta,x)$, in order to examine strength asperity effects on rupture progression, as discussed by Dmowska and Li [1982]. We show some of his results (for uniformity of strength along strike) in a subsequent figure.

However, it appears that when the advance of the rupture front is not strongly nonuniform along strike, so that $\sigma(x,t)$ is nearly uniform in x along $-L < x < +L$ (except, of course, near the ends), a much simpler but approximate analysis can be employed. This is described in the next section and shown later to produce reasonable agreement with Li's results when implemented for the uncoupled case.

Approximate Single Degree of Freedom Description of Deformation and Instability

Here, rather than dealing with point wise along-strike $\sigma(x,t)$ and $\delta(x,t)$ distributions we analyze the stress as if it were uniform along the zone $-L < x < +L$. This zone represents a seismic gap in which upward progressing rupture occurs over the time scale analyzed. Hence we write $\sigma(x,t) = \sigma(t)$ for x within the gap zone, and if $\sigma_0(x,t) = \sigma_0(t)$ also within this zone, the cut of length 2L in Figure 1c can be regarded as a crack in a two-dimensional Elsasser sheet subject to uniform stress drop $\sigma_0 - \sigma$. The relative displacement $\delta(x,t)$ of the crack surfaces, given by solving the Elsasser plate equations, is then not strictly uniform along strike. But to retain simplicity, we define $\delta(t)$ as the average of $\delta(x,t)$ over the gap zone $-L < x < +L$, and we further insist that the constitutive relation $\sigma = f(\delta)$, descriptive of rupture progression at a representative section, applies so as to relate $\sigma(t)$ to $\delta(t)$. The result is to reduce effectively the model of rupture progression to a single degree of freedom system.

Considering a stress drop $\sigma_0(t) - \sigma(t)$ along a crack of length 2L in the generalized Elsasser plate and recognizing that the plate is visco-elastic, it is clear that the resulting $\delta(t)$ can be given by the representation

$$\delta(t) = \int_{-\infty}^{t} C(t-t') \frac{d}{dt'} [\sigma_0(t') - \sigma(t')] \, dt' \qquad (13)$$

This is just the single degree of freedom version of (9), but now with δ expressed in terms of $\sigma_0 - \sigma$ rather than the converse; $C(t)$ is the compliance of the generalized Elsasser plate and represents the (average) slip displacement along a

crack of length 2L at time t due to imposition of a uniform, unit stress drop on the crack surfaces at time $t = 0$. A Laplace transform expression for $C(t)$ developed from the approximate simulation of a finite crack by Lehner et al. [1981] is given by equation (B7) in Appendix B and used for our calculations here.

When the relation $\sigma = f(\delta)$ describing rupture progression is additionally imposed, (13) becomes an integral equation describing the evolution of $\delta(t)$ in response to a given tectonic stress variation $\sigma_0(t)$. It is straightforward to understand the general nature of the solutions when the relation $\sigma = f(\delta)$ has a form like that shown in Figure 2.

Consider first the regime for which all stress and displacement variations are sufficiently slow that coupling of the elastic lithosphere to the asthenosphere may be neglected, i.e., for which the time scale is long compared to the relaxation time of the cracked Elsasser plate. In this case the source of time-dependent compliance is irrelevant and (13) simplifies to

$$\delta(t) = C(\infty)[\sigma_0(t) - \sigma(t)] \qquad (14)$$

Here $C(\infty)$, the longtime compliance, corresponds to that of a cracked plate decoupled from its foundation. It is given by (Appendix B)

$$C(\infty) = 8L/\pi(1+\nu)G \qquad (15)$$

Equation (14) is related to (13) as is (12) to (9). With reference to Figure 2, (14) shows that σ and δ are constrained to lie on a line of slope $-1/C(\infty)$ cutting the stress axis at σ_0. Since σ and δ must likewise satisfy the relation $\sigma = f(\delta)$, the system traverses states A, B, etc. shown as $\sigma_0(t)$ increases through the values at A', B', etc. Point I represents the instability point or at least what would be the instability point if the lithosphere were actually decoupled from the asthenosphere.

The situation developing in the vicinity of point I is a familiar one, closely analogous to instability analyses developed by Rice [1979] and Rice and Rudnicki [1979] for cases in which pore fluids provide a source of unrelaxed constitutive response. In the present case the high rates of δ predicted in the vicinity of point I imply that coupling to the asthenosphere can no longer be neglected. The viscoelastic integral relation of (13) is then followed rather than its relaxed limit in (14), and the system can be considered to be self-driven when σ_0 exceeds the value at I'. This is because no relaxed equilibrium state can then exist, even if σ_0 is held constant, as is obvious from the graphical construction, and the imposed load can be supported only by continual creep motion so as to generate supporting stresses of viscous origin.

To characterize final instability of this range of self-driven quasi-static response, observe that increments of δ and σ corresponding to very rapid deformation are related by

$$d\sigma = -C(0)d\delta \qquad (16)$$

where $C(0)$ is the unrelaxed, or instantaneous, compliance of the lithosphere-asthenosphere system. It corresponds to full coupling of the lithosphere

to the asthenosphere, with the latter undergoing only instantaneous elastic response. It is given by (Appendix B)

$$C(0) = \frac{H^2}{(1+\nu)LG} \int_0^{2L/H} [erf\sqrt{\phi}]^2 \, d\phi \qquad (17)$$

and, of course, $C(0) < C(\infty)$. Hence, no further quasi-static solution exists when the system deforms beyond the point labeled D in Figure 2, at which the slope of the relation $\sigma = f(\delta)$ equals $-1/C(0)$. Thus point D marks the point of dynamic instability for the system, which we take to be the analog of a great crustal earthquake.

The self-driven transition range from I to D is one in which rapid increases of deformation in time are expected. This is confirmed by detailed calculations in a future paper (V. C. Li and J. R. Rice, unpublished manuscript, 1983), which focuses on the time evolution of slip zone progression implied by our model and on the associated time-dependent precursory surface strains. While the thickness-averaged stress σ is decreasing in the postpeak range before instability, stress and strain near the fault trace at the earth's surface increase rapidly in time by comparison to rates well prior to instability, since the origin of the slip softening in Figure 2 is the progression of the ruptured zone toward the earth's surface.

The discussion thus far has been carried out on the presumption that $f(\delta)$ actually has a form like that shown in Figure 2. The form in that figure has, in fact, been drawn to comply with the elastic-brittle crack model of rupture progression, derived in the next section. But the relation $f(\delta)$ is dependent on the way that rupture is modeled, and it is evident, e.g., from results of σ versus δ presented by Stuart and Mavko [1979, Figures 2 and 3] for their slip-weakening model of a plate boundary, that the geometry of the curve $\sigma = f(\delta)$ may be altered greatly by variation of the parameters that describe the slip-weakening process and its depth dependence. The appearance of a peak in $f(\delta)$, beyond which softening occurs, would seem to be a general feature. But it is possible for some range of parameters that the slope $f'(\delta)$ never falls beneath $-1/C(\infty)$, in which case the rupture process is completely stable and would be even in the absence of asthenospheric coupling. In that case, no point like I is encountered, and rupture or slip of the gap zone is accomplished aseismically. Alternatively, it may be possible that $f'(\delta)$ falls below $-1/C(\infty)$ over some range of δ but never falls below $-1/C(0)$. In this case, dynamic, or seismic, instability is not possible, but the self-driven creep range is entered, and this may be detected as a relatively rapid but aseismic deformation event at the earth's surface.

Finally it should be recalled that $\sigma(t)$ is expressible as a direct function of $\delta(t)$, as in Figure 2, rather than as a functional of prior $\delta(t')$, $-\infty < t' \le t$, only when the rupture process at the plate boundary is considered to be described locally by time and rate insensitive deformation and fracture properties. Such descriptions are plainly of an approximate character. They are not general enough to include fault surface healing or other processes of restrengthening in relaxational contact, as required of any description versatile

enough for arbitrary numbers of consecutive rather than just single great earthquake cycles.

Elastic-Brittle Crack Model of Rupture Progression

Here we derive the relation $\sigma = f(\delta)$ on the assumption that the rupture process depicted in Figure 1b can be described by elastic-brittle crack mechanics. In this case the local antiplane shear stress τ_{yx} on the plate boundary vanishes over the ruptured segment $H - a < z < H$ (we may measure local stress from zero at its value at the end of the previous earthquake cycle). The boundary is unslipped for $0 < z < H - a$. Advance of the slip zone occurs when the crack tip energy release rate $\mathscr{G}$, expressible in terms of the mode III crack tip stress intensity factor

$$K \equiv \lim_{z \to (H-a)^-} \{\sqrt{2 \ (H-a-z)} \, \tau_{yx}(z, y = 0)\} \qquad (18)$$

by

$$\mathscr{G} = K^2/2G \qquad (19)$$

attains a critical value $\mathscr{G}_c$. We assume that $\mathscr{G}_c$ varies with depth or, as is equivalent, that $\mathscr{G}_c = \mathscr{G}_c(a)$.

The mode III solution for an edge crack of depth a in an elastic strip is well known [Paris and Sih, 1965; Tada et al., 1973] and the stress intensity factor is

$$K = \sigma\sqrt{2H \ \tan(\pi a/2H)} \qquad (20)$$

Further, from the analysis of this solution by Tada et al. [1973, section 2.5] the thickness-averaged slip δ (which Tada et al. call Δ) at the ruptured boundary, which is interpretable alternately as that part of the remote shear displacement of one side of the strip in Figure 1b relative to the other due to the presence of the rupture, and the local relative slip w_b (which Tada et al. call δ) at the base of the lithosphere are

$$\delta = (4\sigma H/\pi G)\ln[1/\cos(\pi a/2H)]$$
$$w_b = (4\sigma H/\pi G)\cosh^{-1}[1/\cos(\pi a/2H)] \qquad (21)$$

Thus by requiring that σ be of magnitude that just meets the fracture advance criterion at crack depth a, we obtain

$$\sigma = [G\mathscr{G}_c(a)/H \ \tan(\pi a/2H)]^{1/2}$$
$$\delta = (4H/\pi G)[G\mathscr{G}_c(a)/H \ \tan(\pi a/2H)]^{1/2} \qquad (22)$$
$$\times \ln[1/\cos(\pi a/2H)]$$

These two equations together constitute a relation $\sigma = f(\delta)$, as in (10) and Figure 2, where the relation is expressed parametrically in terms of crack depth a.

Following Stuart [1979a, b] and Stuart and Mavko [1979], we assume for our subsequent calculations that

$$\mathscr{G}_c(a) = \mathscr{G}_{max} \exp[-(H-a-z_0)^2/b^2] \qquad (23)$$

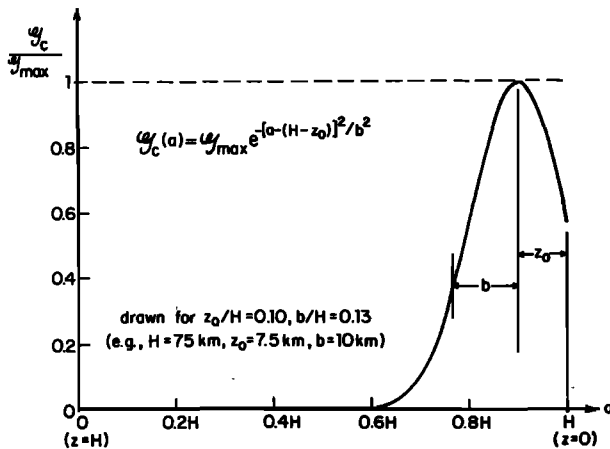This defines (Figure 3) a bell-shaped distribution with peak at depth z_0, which we take to be in the

Fig. 3. Assumed fracture energy variation.

range of 5 to 15 km, and variance width $b/\sqrt{2}$ where we take b in the range 5 to 10 km. These choices serve to induce great earthquake instabilities when cracks have propagated aseismically to an extent that their tips are within approximately 5 to 15 km of the earth's surface, i.e., in the seismogenic layer. The maximum $\mathcal{G}_c$, $\mathcal{G}_{max}$, is chosen to make predicted seismic stress drops and slips fall into a range appropriate for great earthquakes, and as supported by our subsequent illustrations, this suggests that we choose $\mathcal{G}_{max} \approx 4 \times 10^6$ J/m^2. (For given z_0 and b, all predicted critical stress levels and stress drops are directly proportional to $\mathcal{G}_{max}^{1/2}$, as is evident from (22).)

This estimate of $\mathcal{G}_{max}$ is consistent as regards order of magnitude with the value 10^7 J/m^2 suggested by Ida [1973] from analysis of strong motion data and coincides with the 4×10^6 J/m^2 estimate made by Rudnicki [1980] in considering plate motion and earthquake recurrence for the San Andreas fault. However, the estimate is considerably higher than laboratory shear fracture values inferred from failure tests on initially intact triaxial specimens sustaining a single macroscopic shear fracture in the postpeak regime. For example, $\mathcal{G}_c$ results summarized by Rice [1980] and Wong [1982] for granites under confining pressures of 50 to 300 MPa (0.5 to 3 kbar) are in the range of 10^4 to 10^5 J/m^2. Perhaps the significantly higher field-based estimates mean that the actual rupture process, although represented mathematically as taking place on a single continuous plane, actually involves several non-coplanar rupture fronts that are separated by more coherent material which must also be broken for rupture advance to take place on the megascale under consideration here.

To make further contact with the slip-weakening description of rupture by Stuart [1979a, b] and Stuart and Mavko [1979], we note that these authors assumed a relation between local shear strength $\tau(=\tau_{yx})$ and local antiplane slip displacement w in the form

$$\tau = \tau(z,w) = S \exp[-(z-z_0)^2/b^2]\exp[-w^2/\lambda^2] \qquad (24)$$

According to the theory of slip-weakening shear failure developed by Ida [1972] and Palmer and

Rice [1973], when λ is sufficiently small, this slip-weakening approach to failure coincides with an elastic-brittle crack model as developed above with

$$\mathcal{G}_c(a) = \int_0^\infty \tau(z=H-a,w) \, dw \qquad (25)$$

i.e., with $\mathcal{G}_{max}$ in (23) given by

$$\mathcal{G}_{max} = S \int_0^\infty \exp(-w^2/\lambda^2) \, dw = \sqrt{\pi} \, S\lambda/2 \qquad (26)$$

Further, according to estimates of the size ω of the zone of strength degradation near the tip of cracklike slip-weakening zone (Palmer and Rice [1973] and Rice [1980], eqs. 6.11 and 6.12 adapted to antiplane strain)

$$\omega \approx (1 \text{ to } 2)G\mathcal{G}_{max}/S^2 \qquad (27)$$

at the peak $\mathcal{G}_c = \mathcal{G}_{max}$, and the elastic-brittle crack approach is justified when ω is small compared to a, $H-a$, and the length scales such as b over which $\mathcal{G}_c$ changes appreciably. We have no highly reliable choice of parameters, but taking $G = 5.5 \times 10^{10}$ Pa, $\mathcal{G}_{max} = 4 \times 10^6$ J/cm^2 as earlier, and $S = 5 \times 10^7$ Pa = 500 bars (note that S should be significantly larger than typical great earthquake stress drops and represents the largest peak strength level, attained very near the rupturing front), we have $\omega \approx 100$ to 200 m from (27) and $\lambda \approx 90$ mm from (26). These numbers are of the order of 200 or so times the corresponding ω and λ values that would be inferred from laboratory fractures [Rice, 1980; Wong, 1982] but the range for ω is still sufficiently small compared to a, $H-a$ and b (all typically greater than several kilometers) that the elastic-brittle crack model would seem to be justified. Still, it must be noted that the parameter choices are uncertain, and, e.g., an estimate of S one fifth as large, $S = 100$ bars, would give ω values 25 times larger (i.e., 2.5 to 5 km) and fall outside of a reasonable range for validity of the elastic-brittle crack approach.

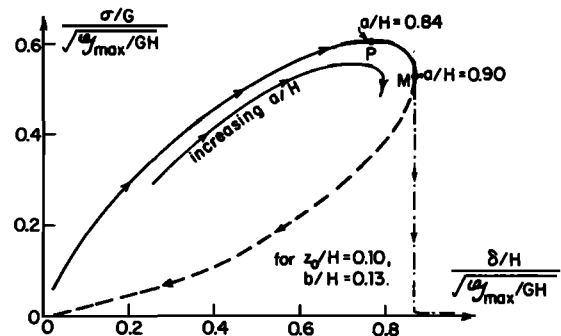The $\sigma = f(\delta)$ relation based on (22) and (23) is shown as Figure 4. The dimensionless stress

Fig. 4. Thickness-averaged stress versus slip relation for elastic-brittle crack model of the antiplane rupture progression depicted in Figure 1b. Based on (22) and fracture energy distribution as in Figure 3 and (23).

and displacement as plotted depend only on a/H, b/H and z_0/H, and since the first of these is just the parameter which generates the curve, the resulting stress-displacement curve depends only on z_0/H and b/H. That drawn, with $z_0/H = 0.10$, $b/H = 0.13$ is consistent, for example, with $z_0 = 7.5$ km, $b = 10$ km in a lithosphere of thickness $H = 75$ km; the shape of the curve is not greatly altered by other z_0 and b choices within the ranges given earlier. Point P marks the peak strength point and corresponds to $a/H = 0.84$ in this illustration. Increase of a/H to 0.90 reaches the point M of maximum displacement. Further increases of a/H toward unity actually correspond to the dashed branch of the curve which loops back toward the origin; this branch is not physically meaningful because it corresponds to extensive back slip on the crack surfaces in the lower portions of the lithosphere. In any event, it is evident from Figure 2 that dynamic instability will occur before point M is reached, and we can think of the actual σ versus δ curve as exhibiting an unstable vertical drop at M, as illustrated by the dashed and dotted line.

The instability points I and D of Figure 2 must lie between points P and M in Figure 4 and thus occur within a range bounded, for the present choice of parameters, by $0.84 < a/H < 0.90$. For $H = 75$ km, this range corresponds to advancing the front of the rupture upward from 12 to 7.5 km below the earth's surface. Hence instability and the associated time-dependent processes that precede it occur over a range of crack length shortly prior to reaching the location of peak fracture resistance in Figure 3, i.e., at 7.5 km depth in this case.

Using $\mathcal{G}_{max} = 4 \times 10^6$ J/m^2 and $G = 5.5 \times 10^{10}$ Pa, $H = 75$ km as previously, the peak value of thickness-averaged stress in the lithosphere in this illustration is $\sigma_p = 1.0 \times 10^6$ Pa = 10 bars; the corresponding average stress on the unruptured ligament, $H-a$, is 62.5 bars. Also, the thickness-averaged slip displacement at the plate boundary at peak strength is $\delta_p = 1.8$ m.

Overall features of the σ versus δ relations implied by (22), for general choices of $\mathcal{G}_c(a)$ possibly different from that in (23), can be found by the following procedure. We define

$$\rho = \rho(a) \equiv \frac{H}{\pi \mathcal{G}_c(a)} \frac{d\mathcal{G}_c(a)}{da} \qquad (28)$$

and plot it versus a/H. For example, this function is represented in Figure 5, with ρ values given along the vertical axis, by the straight line (of negative slope)

$$\rho = (2H/\pi b)\{[(H-z_0)-a]/b\} \qquad (29)$$

corresponding to the bell-shaped $\mathcal{G}_c$ of (23), plotted again for $z_0/H = 0.10$, $b/H = 0.13$. Observe that the ρ versus a/H plot must always cross the level $\rho = 0$ with negative slope at the location of a peak in the fracture energy $\mathcal{G}_c$.
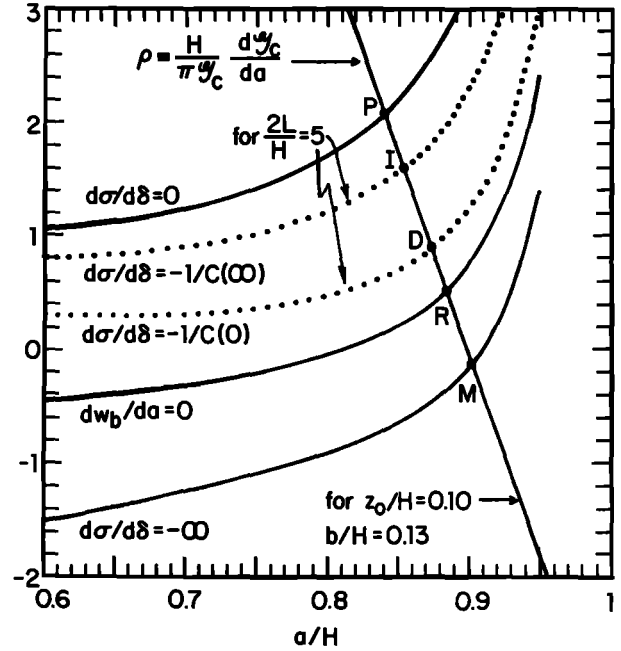
From (22) and the definition of ρ in (28) one

Fig. 5. Procedure for determining dimensionless crack size a/H corresponding to various critical points of σ versus δ relation: P for peak strength, I for initial instability, D for dynamic instability, R for incipient reverse slip at lithosphere base, M for vertical tangent of σ versus δ relation.

may calculate that

$$d\sigma/da = (\pi\sigma/2H)[\rho - 1/\sin(\pi a/H)] \qquad (30)$$

$$d\delta/da = (2\sigma/G)\{[\rho - 1/\sin(\pi a/H)]\ln[1/\cos(\pi a/2H)]$$
$$+ \tan(\pi a/2H)\}$$

Hence it is seen that the peak strength point P, at which $d\sigma/d\delta = 0$, is given by

$$\rho = 1/\sin(\pi a/H) \qquad (31)$$

The right side of this equation plots as the upper solid curve in Figure 5, and its intersection with the plot of ρ versus a/H defines a/H at peak. Similarly, the maximum displacement point M corresponds to $d\sigma/d\delta = -\infty$, which is equivalent to

$$\rho = 1/\sin(\pi a/H) - \tan(\pi a/2H)/\ln[1/\cos(\pi a/2H)] \qquad (32)$$

The right side of this equation plots as the lowest curve in Figure 5 and its intersection with the plot of ρ versus a/H defines a/H at M.

Another point of interest is that for which the crack model first predicts reverse slip. Presumably, the predicted form of the σ versus δ relation loses validity for any greater a/H, since it is expected that a tendency for reverse slip would be resisted by locking of the crack surfaces deep in the lithosphere, and this effect is not included in the calculation leading, e.g., to the σ versus δ relation in Figure 4. The crack surface displacement w_b at the base of the lithosphere is given in (21), and reverse slip first occurs there when $dw_b/da = 0$, which one may show to be equi-

TABLE 1. Depth of Crack Tip at Peak Stress and at Dynamic Instability,
Lithospheric Thickness-Averaged Slip and Stress at Instability,
Estimated Maximum Seismic Slip and Nominal Seismic Stress Drop

| | H=75 km | | | | H=35 km | | | |
| | $z_0=7.5$ km | | $z_0=15$ km | | $z_0=3.5$ km | | $z_0=7$ km | |
	b=5 km	b=10 km	b=5 km	b=10 km	b=5 km	b=10 km	b=5 km	b=10 km
$H-a_p$, km	8.63	11.97	15.97	18.18	5.81	9.60	8.71	12.05
$H-a_D$, km	7.68	9.58	15.32	15.79	4.47	6.03	7.59	8.71
δ_D, m	2.20	2.12	1.90	1.86	1.40	1.24	1.26	1.16
$\sigma_D \equiv \Delta\sigma$, bars	6.86	7.52	9.50	9.52	10.74	11.58	14.12	14.84
w_s, m	4.4	4.2	3.8	3.7	2.8	2.5	2.5	2.3
$\Delta\tau_s$, bars	45	39	31	30	56	45	43	40

Entries based on $\mathscr{G}_{max} = 4 \times 10^6$ J/m^2 and $2L/H = 5$.

valent to

$$\rho = 1/\sin(\pi a/H)$$
$$-1/[\cos(\pi a/2H)]\{\cosh^{-1}[\sec(\pi a/2H)]\} \qquad (33)$$

This equation defines point R in Figure 5, giving the maximum a/H before reverse slip is predicted.

Even though dynamic instability typically occurs before point R is reached for the range of parameters that we have examined here, the tendency for reverse slip may be of considerable importance in determining characteristics of the seismic rupture event itself. In particular, this reverse slip and attendant locking tendency at depth may be important to determining how deeply slip motions extend downward, during the seismic event, beneath the ligament of dimension $H - a_D$ that was still unruptured just before dynamic instability.

The manner of plotting in Figure 5 nicely isolates the effect of any particular assumption about the distribution of critical fracture energy with depth. This distribution affects only the ρ versus a/H plot; the other curves so far discussed are universal, and the additional dotted curves to be discussed soon are universal for a given $2L/H$. Further, as regards the peak and postpeak range of $\sigma = f(\delta)$, only the portion of the ρ versus a/H plot just prior to $\rho = 0$ is significant. From (28), this part of the plot is seen to depend on the variation of $\mathscr{G}_c(a)$ with a just prior to the location of peak fracture resistance.

Instability Conditions Based on Elastic-Brittle Crack Model of Rupture Progression

Instability conditions within the single degree of freedom analysis discussed in connection with Figure 2 are now illustrated. The initial instability point I, beyond which self-driven creep occurs, and the final dynamic instability point D are characterized by

$$d\sigma/d\delta = -1/C \qquad (34)$$

where $C = C(\infty)$, the relaxed, uncoupled compliance of (15), for point I and $C = C(0)$, the instantaneous, fully coupled compliance of (17), for point D. By using (30), satisfaction of (34) is equi-

valent to

$$\rho = \frac{1}{\sin(\pi a/H)} - \frac{\tan(\pi a/2H)}{\ell n[1/\cos(\pi a/2H)]+\pi GC/4H} \qquad (35)$$

This expression contains the term $\pi GC/4H$, and hence to define point I, we write from (15) that

$$\pi GC(\infty)/4H = [2/(1+\nu)](L/H) \qquad (36)$$

and to define D, from (17), that

$$\pi GC(0)/4H = \frac{\pi}{4(1+\nu)} \frac{H}{L} \int_0^{2L/H} [erf\sqrt{\phi}]^2 \, d\phi \qquad (37)$$

Plots of the right side of (35) with the use of (36) and (37), respectively, define the upper and lower dotted curves in Figure 5, presented here for the case $2L/H = 5$ and $\nu = 0.25$. Their intersections with the plot of ρ versus a/H thus defines the instability points I and D, as illustrated.

Note that the instability points I and D occur over a relatively narrow range of a/H, where ρ is falling steeply toward zero. Again, the structure of ρ versus a/H in this range is determined by the form of the rise of fracture resistance toward peak; the remainder of the $\mathscr{G}_c$ versus a relation is not particularly relevant to prediction of instability. (Evidently the elastic-brittle crack model always predicts an instability for any meaningful choice of $\mathscr{G}_c$ variation; this contrasts with predictions of more general slip-weakening models of rupture progression.)

The construction in Figure 5 allows inference of the dependence of the I to D transition on fracture parameters. For example, the ρ illustrated corresponds to a brittle zone thickness $b = 10$ km in a lithosphere with $H = 75$ km. In this case the crack extension from I to D is $a_{I\to D} = 1$ km. But the slope of the ρ line is proportional to $1/b^2$ and hence is steeper for smaller b. Thus for $b = 5$ km one finds $a_{I\to D} = 0.3$ km.

A numerical tabulation of instability results is given in Table 1 for two choices of lithosphere thickness and for several different choices of the depth z_0 to peak strength and width b of the brittle zone. The first row shows the depth $H-a_p$ to the crack tip at peak strength and the second

the depth $H-a_D$ at onset of the final seismic in-
stability. The second row and further entries in
the table depend on the along-strike size of the
rupturing zone but only slightly so when $2L/H$ is
large since the right side of (37) approaches the
constant value $\pi/2(1+\nu)$ at large $2L/H$; the table
is based on $2L/H = 5$. The third and fourth rows
show the lithospheric thickness averaged slip δ_D
at final instability and the thickness-averaged
stress σ_D, which we equate to the drop $\Delta\sigma$ in
the thickness-averaged stress during the earth-
quake. The entries in the third and fourth rows
are directly proportional to $\mathcal{G}_{max}^{1/2}$; the numerical
values are given for $\mathcal{G}_{max} = 4 \times 10^6$ J/m^2.

Since our model does not describe the seismic
rupture itself, some estimates must be made of the
associated values of seismic slip w_s at and near
the earth's surface and of the nominal seismic
stress drop $\Delta\tau_s$, as conventionally reported. To
estimate w_s simply, we note that just prior to
instability the plate boundary is still locked
against slip in the near-surface region and has
maximum relative slippage w_b near the base of
the lithosphere. From the expressions for w_b
and δ in (21), $(w_b)_D \approx 1.5 \delta_D$ for a_D/H in
the vicinity of 0.85, which is typical. We should
also recognize that δ_D as it enters the one
degree of freedom model represents an average slip
over the rupture length $2L$. Assuming for simplic-
ity that the actual slip profile is of elliptical
form along strike, the maximum slip is approxi-
mately 1.5 times the average, and hence the maximum
base slip w_b just before instability is
approximately $2\delta_D$. If it is now assumed that the
seismic event involves the near-surface portions
of the plate boundary slipping so as to catch up
with the accumulated slip at its base, we have

$$w_s \approx 2\delta_D \qquad (38)$$

and such results for w_s are given in the fifth
row of Table 1.

To estimate the nominal seismic stress drop
$\Delta\tau_s$, we must convert the thickness-averaged stress
drop $\Delta\sigma$ to one over an appropriate effective area
that can be assumed to slip during the earthquake.
The ligament thickness $H-a_D$, unruptured just
before the event, can be assumed to slip during it.
It would seem untenable, however, to assume that
seismic slip does not also extend below this liga-
ment. Rather arbitrarily, for purposes of assigning
an area over which a nominal stress drop is
reported, we assume that seismic slip extends
downward an effective distance equal to half the
ligament thickness at instability and hence
associate a nominal seismic stress drop with the
event by

$$H\Delta\sigma = (3/2)(H-a_D)\Delta\tau_s \qquad (39)$$

The resulting seismic stress drops are shown in
the last row of Table 1.

The estimates of w_s and $\Delta\tau_s$ thus given
cover a reasonable range for great crustal earth-
quakes. Of course, both are proportional to $\mathcal{G}_{max}^{1/2}$,
and the 4×10^6 J/m^2 value has been chosen
accordingly. Perhaps any value in the range of 1
to 4×10^6 J/m^2, the lower value halving the w_s
and $\Delta\tau_s$ values from those in the table, could be
considered equally reasonable as a representation

of typical behavior. For example, the average
surface slip is about 3 m for 11 large shallow
earthquakes listed by Geller [1976] with seismic
moment $M_0 \geqslant 15 \times 10^{27}$ dyne cm, with the exception
of the Chilean earthquake, which has an exception-
ally long rupture length. Also, the same 11
events give an average value of about 30 bars for
stress drop, and Kanamori and Anderson [1975]
suggest this value as being typical of interplate
earthquakes.

Our model implies an approximate insensitivity
of the nominal stress drop to the surface length
$2L$ of the rupture. This is because the stress
drop depends only on the parameters of point D.
As remarked, the instantaneous elastic compliance
which enters into the calculation of point D in
Figure 5 and (35) and (37) becomes insensitive to
$2L$ for large rupture length, but there is not a
strong variation even for a much shorter rupture
length such as $2L/H = 1$. Consider, for example,
the case $H = 75$ km, $b = 10$ km, $z_0 = 7.5$ km. For
$2L/H = 5$, as in Figure 5 and Table 1, we obtain
$H-a_D = 9.58$ km and $\Delta\tau_s = 39$ bars. When the same
calculation is done for $2L/H = 1$, there results
$H-a_D = 8.63$ km and $\Delta\tau_s = 41$ bars. Thus for a given
distribution of fracture properties with depth, the
model predicts a nominal seismic stress drop that
is essentially independent of the size along strike
of the gap zone which ruptures.

The seismic slips as we estimate them are like-
wise not strongly dependent on $2L$. However, it
may be the case (as suggested recently by Das
[1982]) that very large 'crustal' earthquakes
actually involve some seismic slip over the entire
lithospheric thickness. In this case, w_s would be
greater than what is necessary merely to catch up
with the preseismic base slip w_b. An analysis of
this possibility is beyond the scope of our work
but, as Das [1982] remarks, it may be a source of
the apparent scaling of w_s with $2L$ discussed
by Scholz [1982].

Comparison With Numerical Solution of Integral Equation for Along-Strike Slip Distribution

Instability predictions in the previous section
have been based on the single degree of freedom
model, introduced as a simple means of understand-
ing phenomena described more accurately by the
integral equation in x and t for $\delta(x,t)$
given by (9) and (10). No full solutions to that
integral equation have yet been computed, but as
mentioned previously, Li [1981] has presented
solutions to the simpler integral equation based
on (12) rather than (9) and corresponding to
rupture progression in an elastic lithosphere that
is decoupled from the asthenosphere.

These solutions were done for the σ versus δ
relation constructed for the elastic-brittle crack
model, equations (22) and (23). The method of
numerical solution involves discretization of the
Cauchy singular integral operator in (12) at
collocation points based on roots of Chebychev
polynomials [Erdogan and Gupta, 1972] and iterative
incremental solution of the resulting nonlinear
discrete system for δ in response to small in-
crements in σ_0, which is taken as uniform along
strike. Full details and a discussion of results,
including those for along-strike fracture strength
asperities (which Li simulated by letting $\mathcal{G}_{max}$
in (23) vary with x), are to be reported elsewhere.

for $\frac{2L}{H} = 5, \frac{z_0}{H} = 0.20, \frac{b}{H} = 0.13$

$$\frac{\mathscr{G}_{max}}{GH} = 2.4 \times 10^{-10}$$
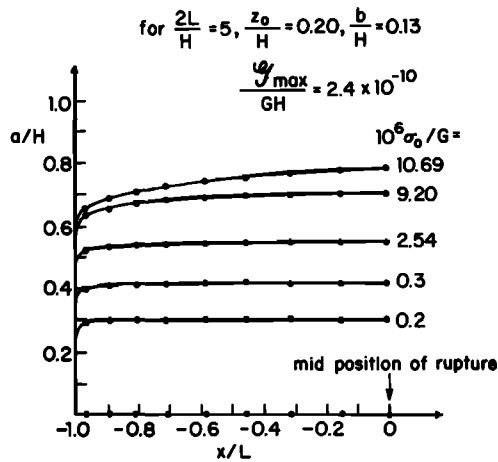
$10^6\sigma_0/G =$

Fig. 6. Results from method of Li [1981], showing successive positions of crack front along strike, for rupture progression by elastic-brittle crack mode in an elastic lithospheric plate that is decoupled from the asthenosphere (i.e., based on numerical solution of the integral equation based on (12) rather than on (9)).

We show in Figure 6 the result of Li's calculation for a case in which fracture properties are uniform along strike, so that there is no explicit x dependence in (10), with the following parameters: $2L/H = 5$, $H = 75$ km, $z_0 = 15$ km, $b = 10$ km, and $\mathscr{G}_{max} = 10^6$ J/m^2. The figure shows successive positions of the fracture front; the number attached to each curve is the value of $10^6\sigma_0/G$. Final instability occurs, in the sense that no further quasi-static solution exists and $\partial\delta(x,\sigma_0)/\partial\sigma_0 \to \infty$, at $10^6\sigma_0/G = 10.7$. At this load the maximum a/H, occurring at the crack center, is 0.78 and the average value of a/H over the middle half of the rupturing zone lies between 0.76 and 0.77 (for the parameters of this problem $a_p/H = 0.757$). Indeed we observe that a/H is fairly uniform along strike, and this implies that σ is also close to uniform.

The last statement lends support to the approximation inherent in our single degree of freedom model, at least in the decoupled case. Instability predictions from the single degree of freedom model can be read from Figure 5, and in this case instability is at point I rather than D since we now compare to calculations for a plate that is decoupled from its foundation. To obtain a/H at instability, we first translate the line representing ρ versus a/H in Figure 5 so that ρ vanishes at 0.8, corresponding to $z_0/H = 0.2$ in the present example rather than 0.1 as in Figure 5. The point I thus determined corresponds to $a/H = 0.772$ at instability, and this is close to the results cited above from Li's calculation. We can compute σ and δ at $a/H = 0.772$ by (22) and (23), and then using (14) with $C(\infty)$ given by (15), we can compute the value of σ_0 at instability. The result is $10^6\sigma_0/G = 11.6$, which differs only by 8% from the result of Li's calculation. The stress prediction is perhaps not that close, however; it may be argued that use of the exact compliance expression (Appendix B) for a cracked plate in plane stress provides the suitable basis for comparison with Li's calcula-

tion, and then we find $a/H = 0.778$ at instability point I and $10^6\sigma_0/G = 13.3$.

Time-Dependent Processes Prior to Instability

As remarked, coupling to the asthenosphere becomes important as instability is approached, and self-driven creep develops after point I is passed. Equation (13) in combination with $\sigma = f(\delta)$, e.g., as constructed from the elastic-brittle crack model, describes this process. The time dependence of the compliance $C(t)$ in (13) is shown by the solid curves in Figure 7 for $2L/H = 1$ and 5. These curves were obtained by numerical inversion of the Laplace transform expression in Appendix B, and

$$h \equiv [C(t) - C(0)]/[C(\infty) - C(0)] \tag{40}$$

is plotted as a function of t/t_r where $t_r \equiv \beta/\alpha$ defines the Maxwell relaxation time of the asthenosphere material.

For most of our numerical work we have used the dashed line approximations to h in Figure 7, which are based on the standard linear model shown as an inset and are given by

$$h = 1 - e^{-t/\gamma t_r} \tag{41}$$

Here $\gamma = 5$ for $2L/H = 1$ and $\gamma = 18.5$ for $2L/H = 5$. The term γt_r corresponds to an effective relaxation time of the coupled plate-asthenosphere system and, assuming $t_r = 5$ years, as previously, this relaxation time is 25 years and 90 years for $2L/H = 1$ and 5, respectively.

The use of similar approximation based on a standard linear model by Rice [1979] and Rice and Rudnicki [1979] for fluid interactions with failing rock was found to lead to numerically close results, and we have found the same in this case. The accuracy was checked by performing limited numerical solutions of the integral equation based on (13) and $\sigma = f(\delta)$ for the elastic-brittle crack model, using the numerically inverted $C(t)$ given by the solid curves in Figure 7 and by comparing the solution to that using the standard
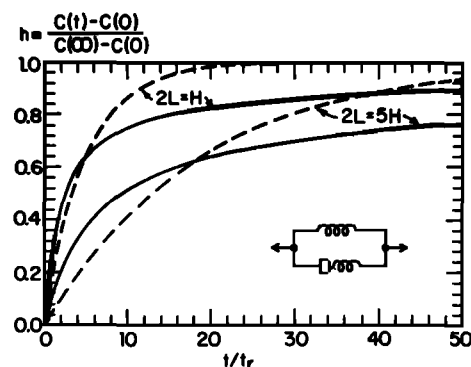

$$h = \frac{C(t)-C(0)}{C(\infty)-C(0)}$$

Fig. 7. Solid lines: time dependence of compliance $C(t)$ of lithosphere-asthenosphere system entering single degree of freedom analysis of rupture progression (equation (13)); $t_r = \beta/\alpha$ is the Maxwell relaxation time of asthenosphere material. Dashed lines: approximations based on fit by standard linear model.

linear mode approximation. The latter procedure required much less computer time but gave results for δ versus t, which were typically within 1% for the cases examined, which is remarkable in view of the relatively poor fit in Figure 7.

When the standard linear model approximation is used for C(t), (13) may be rewritten as the differential equation:

$$\gamma t_r \frac{d}{dt} [\delta - C(0)(\sigma_0 - \sigma)] + [\delta - C(\infty)(\sigma_0 - \sigma)] = 0 \quad (42)$$

and when $\sigma = f(\delta)$ is written, e.g., representing the elastic-brittle crack relation defined by (22) and (23), this becomes a nonlinear equation of first order for $d\delta/dt$ expressed as a function of δ, σ_0, and $\dot{\sigma}_0$, where σ_0 is a prescribed function of time. We start-off solutions at peak strength or sometimes at an earlier crack size a_0 (it seems to make no significant change in results) by assuming that the system is completely relaxed at the start, i.e., that the initial values of σ_0, σ, and δ are related as along A'A in Figure 2, and then we set $d\sigma_0/dt = \dot{\sigma}_0 = $ constant henceforth and integrate forward.

In the solution procedure it proves most convenient to express both δ and σ parametrically in terms of a by (22) and (23), so that (42) becomes an equation for da/dt, conveniently regarded as one for dt/da. Omitting details, the dimensionless form taken by the equation is

$$\frac{d(t/t_r)}{d(a/H)} = F\left(\frac{a}{H}, \frac{t}{t_r}; R, \frac{a_0}{H}, \frac{z_0}{H}, \frac{b}{H}, \frac{2L}{H}\right) \quad (43)$$

where the parameter R upon which function F depends is a dimensionless measure of tectonic stressing rate given by

$$R = t_r \dot{\sigma}_0 / \sqrt{2G\mathscr{G}_{max}/H} \quad (44)$$

Based on related work (V. C. Li and J. R. Rice, unpublished manuscript, 1983) it may be argued that $\dot{\sigma}_0 = 0.006$ to 0.1 bar/yr is a representative range of thickness-averaged tectonic loading rates for the later portions of a great earthquake cycle, and using $t_r = 5$ years, $\mathscr{G}_{max} = 4 \times 10^6$ J/m^2, and H = 75 km, the range of R is thus 0.001 to 0.02.

Equation (43) has been integrated in a/H starting at peak in several cases, and $(t - t_p)/t_r$ is computed as a/H is increased in incremental steps to a_D/H, the final instability point. Results for the evolution of a with time are shown in Figure 8 for $2L/H = 5$, $b/H = 0.07$, $z_0/H = 0.10$, and for two values of R within the range cited above. Points I and D are marked. The self-driven creep regime initiates at I, and the rate of fracture extension is seen to accelerate in its vicinity and to grow toward large values as the dynamic instability point D is neared. Note that $t_{I \to D}$ is $0.3\ t_r$ and $0.5\ t_r$, i.e., approximately 1.5 years and 2.5 years if $t_r = 5$ years, for the two cases shown. These are much shorter than the effective relaxation time of the coupled lithosphere-asthenosphere system.

Since the crack is accelerating in this transition from I to D, one expects that rates of straining at the earth's surface, near the rupturing plate boundary, will become much larger than
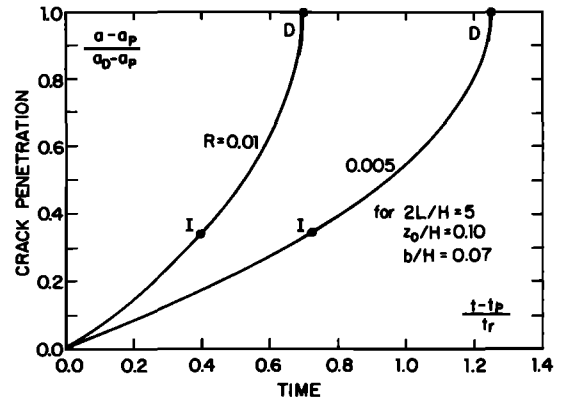

Fig. 8. Time dependence of rupture progression in postpeak regime, based on single degree of freedom analysis with standard linear model fit of viscoelastic compliance and on elastic-brittle crack model of rupture progression.

nominal tectonic strain rates like $\dot{\sigma}_0/G$ during this period. This could have significance for the generation of detectable precursors to the forthcoming instability. A future paper (V.C. Li and J.R. Rice, unpublished manuscript, 1983) presents an extensive analysis of this time dependence and of the surface deformation patterns in space and time implied by the model. For example, we estimate that the time scale of distinct precursory increase in surface deformation rate for the two cases shown in Figure 8, based on $2L/H = 5$ and other parameters as cited above, would be about 10 months for the slower loading rate $R = 0.005$ and about 5 months for the faster $R = 0.01$. The time scales are shorter for smaller along-strike lengths of the rupture, mainly because point I moves closer to D in that case. For example, estimated periods of accelerated precursory strain rate for $2L/H = 1$ and other parameters as above are about 6.5 months for $R = 0.005$ and 3.5 months for $R = 0.01$. For a given $2L/H$, the predicted precursor times are found to vary roughly in proportion to $R^{-1.3}$ over the practical range.

Concluding Discussion

We have presented a general procedure for analysis of large-scale processes of preseismic rupture progression through the lithosphere. The approach is based on the 'line spring' concept of fracture mechanics for part-through ruptures in elastic plates. It is extended here to include coupling, within the Elsasser model, to a viscoelastic asthenosphere and, at least in the general form represented by (9) and (10), is open to the inclusion of various concepts of the physics and geometry of preseismic plate boundary deformation processes and of along-strike variations of strength and tectonic stressing. The approach is developed for transform boundaries but could perhaps be extended to thrust or subduction zones at converging plate boundaries.

Major implications of our modeling include the distinction between instability conditions for an asthenosphere-coupled versus decoupled lithosphere and the importance of the coupling in determining
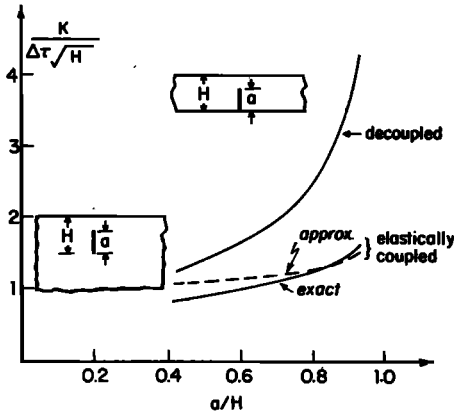
Fig. 9. Stress intensity factors at the upper ends of mode III (antiplane) cracks in elastic lithospheric plates sustaining uniform stress drops $\Delta\tau$. Upper curve: exact result when plate is decoupled from foundation, which result also coincides with prediction by line spring concept. Lower curves: exact (solid, based on two-dimensional elasticity solution for crack in half space) and approximate (dashed, based on line spring concept with Elsasser plate coupled to elastic foundation) results when the lithospheric plate is attached to an elastic asthenosphere of identical elastic modulus.

time-dependent processes of accelerating crustal deformation prior to great earthquake instabilities.

A specific, quantitative description of pre-seismic rupture progression has been developed for the elastic-brittle crack model with a distribution of critical fracture energy that exhibits a peak in the seismogenic layer. This model certainly oversimplifies the physics and local geometry of rupture progression, but we have shown that with plausible choice of model parameters it is possible to produce reasonable predictions of hypocentral depths, seismic slips, and stress drops in great crustal earthquakes. Hence the model seems worthy of further examination as a basis for interpretation of precursory deformation processes. It may also serve usefully as a starting point for inclusion of such effects as rehealing and other rate dependence in rupture progression and for analysis of the effects on rupture progression, and perhaps associated seismicity patterns, of along-strike nonuniformities of strength and tectonic stressing.

Appendix A

To evaluate the accuracy of our extension of the line spring concept in the case of an elastic lithospheric plate that is coupled to an elastic asthenosphere of identical modulus, we consider the mode III crack problem shown by the lower insert in Figure 9 and representing a crack on the surfaces of which there is a uniform stress drop $\Delta\tau$.

The exact expression for the stress intensity factor at the upper crack tip, based on the two-dimensional antiplane strain elasticity solution is [Tada et al., 1973]

$$K/\Delta\tau\sqrt{H} = \sqrt{[\pi/\alpha(1-\alpha)(2-\alpha)]} \; [E(k)/K(k) - (1-\alpha)^2] \quad (A1)$$

where $\hat{\alpha} = a/H$ and $K(k)$ and $E(k)$ are the first and second, respectively, complete elliptic integrals of modulus $k = \sqrt{\alpha(2-\alpha)}$. The result is shown as the lower solid curve in Figure 9. (The upper solid curve is based on (20) and shows the expression

$$K/\Delta\tau\sqrt{H} = \sqrt{2} \; \tan(\pi\alpha/2) \quad (A2)$$

which is the analogous result for a plate that is decoupled from the asthenosphere.)

Now, for the line spring analysis, the stress drop $\Delta\tau$ causes a K as given by (A2), but it also induces a (negative) thickness-averaged stress σ at the boundary, which causes an additional contribution to K given by (20). Hence

$$K = (\Delta\tau + \sigma)\sqrt{2H} \; \tan(\pi\alpha/2) \quad (A3)$$

To determine σ, observe first that the net thickness-averaged slip at the boundary is given by (21) with σ replaced by $\Delta\tau + \sigma$, so that

$$\delta = [4(\Delta\tau + \sigma)H/\pi G]\ell n[1/\cos(\pi\alpha/2)] \quad (A4)$$

But the relation between σ and δ must also be compatible with the generalized Elsasser model, reducing (from either (5) or (8), which give identical results in the present case) to

$$\beta \; \partial^2 u_x/\partial y^2 = u_x \quad (A5)$$

since there is no x dependence and the foundation is taken to be purely elastic. The solution consistent with boundary slip δ is

$$u_x = (\delta/2)e^{-y/\sqrt{\beta}} \quad (A6)$$

so that

$$\sigma = \sigma_{xy}\big|_{y=0} = G(\partial u_x/\partial y)\big|_{y=0}$$
$$= -G\delta/2\sqrt{\beta} = -2G\delta/\pi H \quad (A7)$$

The last equation can be solved simultaneously with (A4) to determine σ in terms of $\Delta\tau$, and when the result is substituted into (A3), there results

$$K/\Delta\tau\sqrt{H} = \frac{\sqrt{2} \; \tan(\pi\alpha/2)}{1+(8/\pi^2)\ell n[1/\cos(\pi\alpha/2)]} \quad (A8)$$

This approximate result based on the line spring modeling is shown by the dashed curve in Figure 9. Its difference from the exact result is not very large, at least for the deep crack lengths of interest in modeling near-surface instabilities.

Appendix B

Let

$$\hat{f}(s) = \int_0^\infty f(t)e^{-st} \; dt \quad (B1)$$

denote Laplace transform of $f(t)$ and observe that after transformation, (2) to (8), relating $\hat{\sigma}_{ij}$, $\hat{u}_i$, and $\hat{\tau}_i$, are formally identical to those of an elastic sheet in plane stress that is coupled

elastically to a foundation with spring constant κ, i.e., $\hat{\tau}_i = \kappa \hat{u}_i$, where $\kappa = HG/(\beta+\alpha/s)$.

Now consider a crack of length $2L$ in the sheet, with uniform 'stress' drop $\Delta\hat{\sigma}(s)$ prescribed along the crack line. It is elementary to see that the leading singularity term in $\hat{\sigma}_{ij}(x,y,s)$ at the tip has the same inverse square root functional form as for classical elastic plane stress (this form is determined by the highest-order terms in the differential equations transformed from (5) or (8) for $\hat{u}_i$; these terms are independent of the presence of the foundation). Thus a quantity K_* analogous to a crack tip stress intensity factor and taking the form

$$K_* = k(2L,s)\Delta\hat{\sigma}(s) \qquad (B2)$$

may be defined. Further, by following Irwin's [1960] classical arguments, one may first observe that a quantity analogous to a crack tip energy release rate (with 'energy' now defined quadratically in terms of Laplace transform quantities and having density

$$\frac{1}{2}\left(\sum_{i,j=x,y} H\hat{\sigma}_{ij}\,\partial\hat{u}_i/\partial j + \sum_{i=x,y}\hat{\tau}_i\hat{u}_i\right)$$

per unit area of the sheet) is given in terms of K_* by the usual elastic plane-stress expression $K_*^2/2(1+\nu)G$; this arises from the 'work' of removing inverse square root singular 'stresses' over incremental distance $d(2L)$ in crack extension from $2L$ to $2L+d(2L)$, and thus the form of the expression is unaffected by presence of the foundation. Next, one observes that Irwin's relation between energy release rate and compliance derivative applies as well in terms of the analogous transformed quatntities, so that if $\hat{\delta}(s)$ is the average 'slip' over the crack length $2L$, then

$$\frac{1}{2}\Delta\hat{\sigma}\left[\frac{\partial(2L\hat{\delta})}{\partial(2L)}\right]_{\Delta\hat{\sigma}\text{ fixed}} = \frac{K_*^2}{2(1+\nu)G} = \frac{k^2(\Delta\hat{\sigma})^2}{2(1+\nu)G} \qquad (B3)$$

Thus

$$\hat{\delta}(s) = \left\{\frac{1}{2(1+\nu)GL}\int_0^{2L}[k(2L',s)]^2 d(2L')\right\}\Delta\hat{\sigma}(s) \qquad (B4)$$

But the relation between $\hat{\delta}(s)$ and $\Delta\hat{\sigma}(s)$ can also be written as $\hat{\delta}(s) = s\hat{C}(s)\Delta\hat{\sigma}(s)$ by using the representation of (13) and transforming both sides; $\Delta\sigma$ represents $\sigma_0 - \sigma$. Comparing to (B4), we derive that

$$\hat{C}(s) = \frac{1}{2(1+\nu)GLs}\int_0^{2L}[k(2L',s)]^2 d(2L') \qquad (B5)$$

Lehner et al. [1981] solve the crack problem for the generalized Elsasser model in the transform domain, using the model (8), and simulating approximately a crack of length $2L$ (they used the notation L where we use $2L$ here) having uniform stress drop as a semi-infinite crack having uniform stress drop over distance $2L$ behind the tip and zero stress drop at greater distances. They obtain (their eq. 42 with L

replaced by $2L$)

$$k(2L,s) = \sqrt{2/\lambda(s)}\ \mathrm{erf}(\sqrt{2L\lambda(s)}) \qquad (B6)$$

where $\lambda(s) = 1/(1+\nu)\sqrt{\beta+\alpha/s}$, and thus the transformed compliance is

$$\hat{C}(s) = \frac{2}{(1+\nu)GLs\lambda(s)}\int_0^{L}[\mathrm{erf}(\sqrt{2\lambda(s)L'})]^2\,dL' \qquad (B7)$$

The long and short time limits of the corresponding function $C(t)$ are given by the limits of $s\hat{C}(s)$ as $s \to 0$ and ∞, respectively, resulting in (15) and (17). The full time variation of $C(t)$ shown in Figure 7 is obtained by numerical inversion [Li, 1981]. We have observed that $(1+\nu)\sqrt{\beta} = (1+\nu)\pi H/4 \approx H$ for the chosen $\nu = 0.25$.

The Lehner et al. approximate simulation of the finite crack leads to a long time compliance $C(\infty)$, given in (15), which is actually $16/\pi^2$ times the exact result in that limit; the exact result is equal to $s\hat{C}(s)$ of (B5) when the well-known stress intensity expression $k = \sqrt{\pi L}$ for an uncoupled plate with crack of length $2L$ is used. Of course, the Lehner et al. [1981] simulation of a finite crack is expected to be least accurate in this uncoupled limit but more accurate when there is substantial coupling to the foundation because then the poorly modeled state at the other end of the crack becomes irrelevant. A way of compensating for this, which we have not appealed to in the discussion within the paper, is to use the Lehner et al. simulation for a rupture length $2L$ which is understood to be $\pi^2/16$ times the actual length.

References

Cathles, L. M., The Viscosity of the Earth's Mantle, Princeton University Press, Princeton, N.J., 1975.

Das, S., Appropriate boundary conditions for modelling very long earthquakes and physical consequences, Bull. Seismol. Soc. Am., 72, 1911-1926, 1982.

Delale, F., and F. Erdogan, Application of the line-spring model to a cylindrical shell containing a circumferential or axial part-through crack, J. Appl. Mech., 49, 97-102, 1982.

Dmowska, R., and V. C. Li, A mechanical model of precursory source processes for some large earthquakes, Geophys. Res. Lett., 9, 393-396, 1982.

Elsasser, W. M., Convection and stress propagation in the upper mantle, in The Application of Modern Physics to the Earth and Planetary Interiors, edited by S. K. Runcorn, pp. 223-246, Wiley Interscience, New York, 1969.

Erdogan, F., and G. D. Gupta, On the numerical solution of singular integral equations, Q. Appl. Math., 29, 525-534, 1972.

Geller, R. J., Scaling relations for earthquake source parameters and magnitudes, Bull. Seismol. Am., 66, 1501-1523, 1976.

Ida, Y., Cohesive force across the tip of a

longitudinal shear crack and Griffith's specific surface energy, J. Geophys. Res., 77, 3796-3805, 1972.

Ida, Y., The maximum acceleration of seismic ground motion, Bull. Seismol. Soc. Am., 63, 959-968, 1973.

Irwin, G. R., Fracture mechanics, in Structural Mechanics, edited by J. N. Goodier and N. J. Hoff, p. 557, Pergamon, New York, 1960.

Kanamori, H., and D. L. Anderson, Theoretical basis of some empirical relations in seismology, Bull. Seismol. Soc. Am., 65, 1073-1095, 1975.

Lehner, F. K., V. C. Li, and J. R. Rice, Stress diffusion along rupturing plate boundaries, J. Geophys. Res., 86, 6155-6169, 1981.

Li, V. C., Stressing processes associated with great crustal earthquakes at plate boundaries, Ph.D. thesis, Brown University, Providence, R.I., 1981.

Nur, A., Rupture mechanics of plate boundaries, in Earthquake Prediction, An International Review, Maurice Ewing Ser., vol. 4, edited by D. W. Simpson and P. G. Richards, pp. 629-634, AGU, Washington, D.C., 1981.

Palmer, A. C., and J. R. Rice, The growth of slip surfaces in the progressive failure of overconsolidated clay slopes, Proc. R. Soc. London, Ser. A, 332, 527-548, 1973.

Paris, P. C., and G. C. Sih, Stress analysis of cracks, ASTM Spec. Tech. Publ., 381, 30-81, 1965.

Parks, D. M., The inelastic line spring: Estimates of elastic-plastic fracture mechanics parameters for surface-cracked plates and shells, Trans. ASME, J. Pressure Vessel Technol., 103, 246-254, 1981.

Parks, D. M., R. R. Lockett, and J. R. Brockenbrough, Stress intensity factors for surface cracked plates and cylindrical shells using line-spring finite elements, in 1981 Advances in Aerospace Structures and Materials - AD-01, edited by S. S. Wang and W. J. Renton, pp. 279-285, American Society of Mechanical Engineers, New York, 1981.

Prescott, W. H., and A. Nur, The accommodation of relative motion at depth on the San Andreas fault system in California, J. Geophys. Res., 86, 999-1004, 1981.

Rice, J. R., The line spring model for surface flaws, in The Surface Crack: Physical Problems and Computational Solutions, edited by J. L. Swedlow, pp. 171-185, American Society of Mechanical Engineers, New York, 1972.

Rice, J. R., Theory of precursory processes in the inception of earthquake rupture, Gerlands Beitr. Geophys., 88, 91-127, 1979.

Rice, J. R., The mechanics of earthquake rupture, in Physics of the Earth's Interior, edited by A. M. Dziewonski and E. Boschi, pp. 555-649, Italian Physical Society/North Holland, Amsterdam, 1980.

Rice, J. R., and N. Levy, The part through surface crack in an elastic plate, J. Appl. Mech., 39, 185-194, 1972.

Rice, J. R., and J. W. Rudnicki, Earthquake precursory effects due to pore fluid stabilization of a weakening fault zone, J. Geophys. Res., 84, 2177-2193, 1979.

Rudnicki, J. W., Fracture mechanics applied to the earth's crust, Annu. Rev. Earth Planet. Sci., 8, 489-525, 1980.

Savage, J. C., and R. O. Burford, Geodetic determination of relative plate motion in central California, J. Geophys. Res., 78, 832-845, 1973.

Scholz, C. H., Scaling laws for large earthquakes: Consequences for physical models, Bull. Seismol. Soc. Am., 72, 1-14, 1982.

Stacey, F. D., Physics of the Earth, 2nd ed., John Wiley, New York, 1977.

Stuart, W. D., Strain softening prior to two-dimensional strike slip earthquakes, J. Geophys. Res., 84, 1063-1070, 1979a.

Stuart, W. D., Strain softening instability model for the San Fernando earthquake, Science, 203, 907-910, 1979b.

Stuart, W. D., and G. M. Mavko, Earthquake instability on a strike slip fault, J. Geophys. Res., 84, 2153-2160, 1979.

Sykes, L. R., and R. C. Quittmeyer, Repeat times of great earthquakes along simple plate boundaries, in Earthquake Prediction, An International Review, Maurice Ewing Ser., vol. 4, edited by D. W. Simpson and P. G. Richards, pp. 217-247, Washington, D.C., 1981.

Tada, H., P. C. Paris, and G. R. Irwin, The Stress Analysis of Cracks Handbook, Del Research Corp., Hellertown, Pa., 1973.

Turcotte, D. L., and D. A. Spence, An analysis of strain accumulation on a strike slip fault, J. Geophys. Res., 79, 4407-4412, 1974.

Wong, T.-F., Shear fracture energy of Westerly granite from post-failure behavior, J. Geophys. Res., 87, 990-1000, 1982.